

Pressure-induced structural modifications of rare-earth hafnate pyrochlore

Katlyn M Turner^{1,4}, Dylan R Rittman¹, Rachel A Heymach¹,
Cameron L Tracy¹, Madison L Turner², Antonio F Fuentes³, Wendy L Mao¹
and Rodney C Ewing¹

¹ Geological Sciences, Stanford University Stanford, CA 94305, United States of America

² Geology, University of Maryland, College Park, MD 20742, United States of America

³ Cinvestav Unidad Saltillo, Apartado Postal 663, Saltillo 25000, Coahuila, Mexico

E-mail: katlynmt@stanford.edu

Received 14 February 2017, revised 20 April 2017

Accepted for publication 5 May 2017

Published 25 May 2017



CrossMark

Abstract

Complex oxides with the pyrochlore ($A_2B_2O_7$) and defect-fluorite ($(A,B)_4O_7$) structure-types undergo structural transformations under high-pressure. Rare-earth hafnates ($A_2Hf_2O_7$) form the pyrochlore structure for $A = \text{La–Tb}$ and the defect-fluorite structure for $A = \text{Dy–Lu}$. High-pressure transformations in $A_2Hf_2O_7$ pyrochlore ($A = \text{Sm, Eu, Gd}$) and defect-fluorite ($A = \text{Dy, Y, Yb}$) were investigated up to ~ 50 GPa and characterized by *in situ* Raman spectroscopy and synchrotron x-ray diffraction (XRD). Raman spectra at ambient pressure revealed that all compositions, including the defect-fluorites, have some pyrochlore-type short-range order. *In situ* high-pressure synchrotron XRD showed that all of the rare earth hafnates investigated undergo a pressure-induced phase transition to a cotunnite-like (orthorhombic) structure that begins between 18 and 25 GPa. The phase transition to the cotunnite-like structure is not complete at 50 GPa, and upon release of pressure, the hafnates transform to defect-fluorite with an amorphous component. For all compositions, *in situ* Raman spectroscopy showed that disordering occurs gradually with increasing pressure. Pyrochlore-structured hafnates retain their short-range order to a higher pressure (30 GPa *vs.* < 10 GPa) than defect-fluorite-structured hafnates. Rare earth hafnates quenched from 50 GPa show Raman spectra consistent with weberite-type structures, as also reported for irradiated rare-earth stannates. The second-order Birch–Murnaghan equation of state fit gives a bulk modulus of ~ 250 GPa for hafnates with the pyrochlore structure, and ~ 400 GPa for hafnates with the defect-fluorite structure. $\text{Dy}_2\text{Hf}_2\text{O}_7$ is intermediate in its response, with some pyrochlore-type ordering, based on Raman spectroscopy and the equation of state, with a bulk modulus of ~ 300 GPa. As predicted based on the similar ionic radius of Zr^{4+} and Hf^{4+} , rare-earth hafnates show similar behavior to that reported for rare earth zirconates at high pressure.

Keywords: oxides, high pressure, pyrochlore

(Some figures may appear in colour only in the online journal)

Introduction

Pyrochlore-structured oxides ($A_2B_2O_7$) and their derivative structures have been extensively studied under the extreme conditions of high pressure [1–11], high temperature [12–15],

and under irradiation [16–37]. The structural transitions that result from extreme environments have been of great interest for pyrochlore-type materials [38]. Pyrochlore-structured materials have been proposed for applications such as hosting immobilized actinides from nuclear fuel reprocessing or dismantled nuclear weapons [39, 40].

The pyrochlore structure ($A_2B_2X_7$; $Fd-3m$) is a $2 \times 2 \times 2$ supercell of the fluorite structure (AX_2 ; $Fm-3m$) in which

⁴ Author to whom any correspondence should be addressed.

359 Green Earth Sciences Building, 367 Panama Street, Stanford, CA 94305, United States of America.

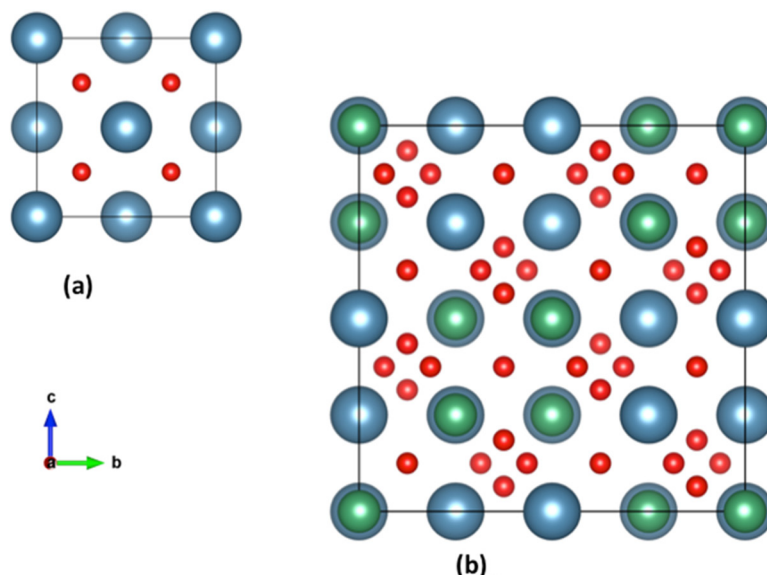


Figure 1. Unit cells of (a) fluorite-type and (b) pyrochlore-type oxides viewed along the [100] direction. In pyrochlore, cation sites are A^{3+} (blue) and B^{4+} (green).

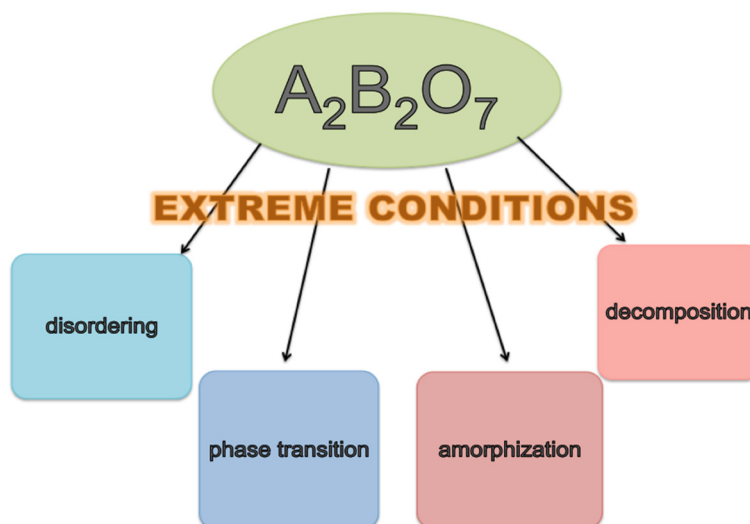


Figure 2. Schematic of structural transformations for $A_2B_2O_7$ pyrochlore under extreme conditions.

there are two ordered cation sites and ordered anion vacancies [41] (figure 1(b)). Larger (often trivalent) cations occupy the $16d$ or A-site in 8-fold scalenohedral coordination, and smaller (often tetravalent) cations occupy the $16c$ or B-site in distorted octahedral coordination [41]. Oxygen anions in the $8b$ site are tetrahedrally coordinated by A^{3+} , the vacant $8a$ site is tetrahedrally coordinated by B^{4+} , and the $48f$ oxygen anions are tetrahedrally coordinated by two each of A^{3+} and B^{4+} [41]. The ratio of cation ionic radii, r_A/r_B , roughly determines whether a material with $A_2B_2O_7$ composition will form the pyrochlore structure. The pyrochlore structure is stable in the r_A/r_B range of 1.46–1.78 [41], though pyrochlore-structured compounds with radius ratio lower than 1.46 can be synthesized via solid-state methods at high temperatures [42, 43].

Materials with $r_A/r_B < \sim 1.46$ form a disordered, defect-fluorite structure [41–57] (figure 1(a)). In defect-fluorite-structured oxides ($Fm-3m$), the A^{3+} and B^{4+} cations are randomly distributed over a single cation site, and all oxygen anions onto one anion site that is $1/8$ vacant, with the vacancies distributed randomly. Recently, Shamblin *et al* investigated the short-to-medium range order of the defect-fluorite structure using neutron total scattering and pair distribution function (PDF) analysis [38]. They found that the defect-fluorite structure consists of local weberite-like orthorhombic units, tessellated such that orthorhombic and isometric fluorite-type structures coexist at different length scales [38]. This analysis was conducted on pyrochlore compounds that had undergone high-energy heavy ion irradiation, but not on pyrochlore compounds that had

Table 1. Cation radius ratio of $A_2Hf_2O_7$ materials [41] ($A = Sm, Eu, Gd, Dy, Y, Yb$).

A	r_A/r_{Hf}
Sm	1.52
Eu	1.50
Gd	1.48
Dy	1.45
Y	1.44
Yb	1.38

disordered through other extreme environments such as high pressure [38].

While many pyrochlore compounds—notably zirconates, titanates, and stannates have been extensively studied under extreme environments [2–38], rare-earth hafnates have received limited attention [1]. Generally, when pyrochlore-structured materials are subjected to extreme conditions, defects are generated by two mechanisms. Anion Frenkel-pairs form, causing the anion sub-lattice to disorder and more closely resemble a defect-fluorite sub-lattice [44, 45, 47–49, 55]. Additionally, anti-site defects form, where A^{3+} and B^{4+} cations disorder [44, 45, 49].

At ambient conditions and at high temperatures, the formation of cation anti-site defects lowers the formation energy of anion Frenkel-pairs. Cation substitution causes all sites to appear similarly electronically on the lattice, and anions can more easily move [44, 45, 47–49]. Under irradiation, disordering of the anion sublattice occurs prior to that of the cation sublattice [50] due to the intrinsic anion vacancies that already exist in the structure. At high pressure, anion disorder tends to occur several GPa lower than cation disorder [2–11]. This is due to the relative ease of ‘oxygen-hopping’ as pressure is applied since a vacancy already exists in the structure. Additionally, BO_6 octahedra can distort to accommodate pressure-induced stress [3]. Both disordering mechanisms occurring simultaneously leads to structural transformations (figure 2).

In extreme environments such as high pressure, high temperature, and under ion irradiation, pyrochlore-type materials have been shown to undergo four types of structural changes [1–38, 50–53] (figure 2). The inherent defect-forming mechanisms in the structure cause disordering from an ordered pyrochlore to a disordered defect-fluorite. Zirconate pyrochlores under high pressure undergo a phase transition to a lower-symmetry cotunnite-like phase ($Pnma$) [2–7, 11, 16, 21, 23, 26, 28, 30, 35]. Some titanate pyrochlores have been shown to become amorphous under high pressure and ion irradiation conditions [6, 9, 10, 19, 24, 26, 51–53], while others have been shown to disorder under ion irradiation to a crystalline defect-fluorite structure [50–53]. Lanthanum hafnate pyrochlore has been shown to decompose to La_2O_3 and HfO_2 under high pressure [1].

The cation radius ratio is the key parameter that determines pyrochlore structural behavior in extreme environments. There may be a relationship between how a given pyrochlore compound reacts to irradiation and high pressure [26]; some pyrochlore compounds that amorphize at high pressure also do so

under ion irradiation. For example, $Gd_2Ti_2O_7$ has a large radius ratio and becomes amorphous at high pressures and under ion irradiation [26]. Rare earth zirconate pyrochlores, which have a smaller radius ratio than titanates, generally form a cotunnite-like structure at high pressure that transforms to defect-fluorite upon quenching [3–7]. Pyrochlore compounds with smaller radius ratios that transform to cotunnite-like structures at high pressure and defect-fluorite upon quenching are more likely to form defect-fluorite under ion irradiation [26].

$Ln_2Hf_2O_7$ pyrochlores ($Ln = La-Tb$) are easily synthesized [41–43, 55]. For $Ln = Dy-Lu$, these compositions have a disordered defect-fluorite structure, although recent work found evidence for pyrochlore domains in $Dy_2Hf_2O_7$ [42, 43]. There is only one study of the high-pressure behavior of a hafnate pyrochlore, $La_2Hf_2O_7$ [1]. In this study, the pyrochlore decomposed into binary oxides: La_2O_3 and HfO_2 , as determined by Raman spectroscopy and powder x-ray diffraction (XRD). This is a surprising result when compared to studies of other pyrochlore compounds at high pressure [2–11]. Although high-pressure experiments have not previously been conducted on other lanthanide hafnate pyrochlores, Zhang *et al* predicted that hafnate pyrochlores would behave similarly to zirconate pyrochlores due to the small radius ratio of Ln^{3+}/Hf^{4+} (table 1) and the similarity in radii of Hf^{4+} and Zr^{4+} [6, 7]. Hafnates are predicted to form the cotunnite-like structure at high pressure, and finally, the disordered defect-fluorite structure upon release of pressure [6, 7]. Here, we present the results of *in situ* Raman spectroscopy and synchrotron XRD experiments investigating the high-pressure structural responses of rare-earth hafnates, $A_2Hf_2O_7$ ($A = Y, Sm, Eu, Gd, Dy, Yb$) to ~50 GPa.

Methods

Samples of $A_2Hf_2O_7$ were synthesized by mechanical ball-milling and high-temperature annealing of HfO_2 and A_2O_3 powders [52]. The precursor powders were mixed in a 2:1 ratio and ball-milled for 24–30 h. The samples were then annealed at 1500 °C for 12 h to eliminate structural defects—cation anti-site defects and anion Frenkel pairs—that accumulate during the ball-milling process [52]. The resulting powders were characterized by powder XRD and Raman spectroscopy at ambient conditions. XRD confirmed that $Sm_2Hf_2O_7$, $Eu_2Hf_2O_7$, and $Gd_2Hf_2O_7$ synthesized as pyrochlore, while $Dy_2Hf_2O_7$, $Yb_2Hf_2O_7$, and $Y_2Hf_2O_7$ formed a defect-fluorite structure (table 1). This is consistent with the prediction based on the radius ratio that rare-earth hafnates ($A = La-Tb$) would form the pyrochlore structure [41–43, 55, 56]. Pyrochlore Raman-active modes are evident in spectra from all samples [57–60] (figure 3), indicating all compositions have some degree of pyrochlore-type short-range ordering.

Samples were loaded into diamond anvil cells (DACs) for *in situ* analysis at high pressure. A symmetric Mao-Bell-type DAC was used with cubic boron nitride and tungsten carbide seats and diamonds with 300 μm culets. Powders were loaded into a stainless-steel gasket with a 120 μm diameter sample chamber. A mixture of methanol and ethanol in a 4:1 ratio

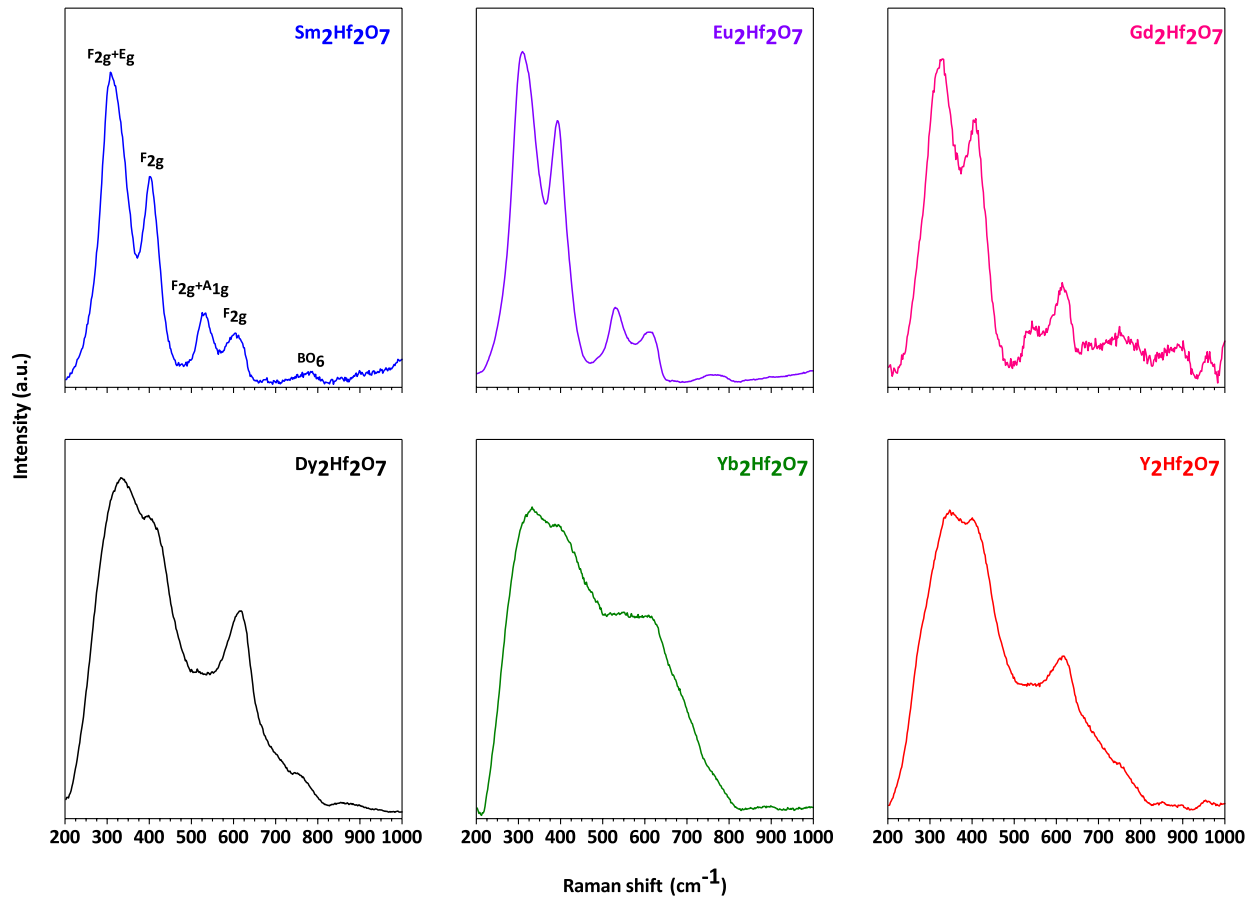


Figure 3. Raman spectra for the suite of rare-earth hafnates at ambient conditions. Spectra of $\text{Sm}_2\text{Hf}_2\text{O}_7$ includes labels for Raman-active modes: $E_g + A_{1g} + 4F_{2g}$, as well as the BO_6 ‘breathing’ mode which is present in all compositions studied.

was used as the pressure-transmitting medium [61, 62]. A ruby sphere was included in the sample chamber to calibrate pressure using the ruby fluorescence method [63]. For Raman spectroscopy and XRD measurements, samples were incrementally compressed to a maximum pressure of 50 GPa, and then quenched to ambient pressure.

In situ high-pressure Raman spectroscopy measurements were collected at Stanford University in the Extreme Environments Laboratory (EEL). A Renishaw RM1000 Raman microscope and 514.5 nm laser was used. The laser power was kept between 10 and 25 mW, and measurements were taken for 90–360 s. The program Fityk was used for spectra analysis and peak fitting [64].

In situ high-pressure powder XRD measurements were collected at beamline 16-BMD of the advanced photon source (APS), and at beamline 12.2.2 of the advanced light source (ALS). X-ray energy varied between experiments from 25 to 40 keV (incident wavelength, $\lambda = 0.4959\text{--}0.3099$ Å). The structures were refined using MAUD software [65]. Parameters refined were the unit cell parameter (a), phase scale factor, microstrain, atom site occupancies, and atomic displacement parameters. The data were refined until convergence was reached in all parameters. Resulting pressure–volume (P – V) data were fit to a second-order Birch–Murnaghan equation of state [66] using EOSFit7GUI software [67]. Errors in the Birch–Murnaghan EOS

Table 2. Fitted peak positions (cm^{-1}) of pyrochlore Raman-active modes in rare earth hafnates ($\text{A}_2\text{Hf}_2\text{O}_7$; A = Sm, Eu, Gd, Dy, Y, Yb) at ambient pressure. Raman peak positions fitted using Fityk [64].

A^{3+}	$F_{2g} + E_g$	F_{2g}	$F_{2g} + A_{1g}$	F_{2g}
Sm	314	403	532	602
Eu	313	393	533	605
Gd	324	410	544	611
Dy	317	414	533	614
Y	324	414	522	614
Yb	309	403	517	617

were propagated from unit cell parameter errors from the refinement.

Results and discussion

Raman spectroscopy was used to characterize the local structure of samples at ambient conditions. Pyrochlore oxides have six theoretical Raman modes [57–60, 68–73]:

$$\Gamma_{\text{Raman}}^{\text{cryst}} = A_{1g} + E_g + 4F_{2g} \quad (1)$$

These Raman-active modes are representative of vibrations of the $\langle\text{Hf-O}\rangle$ and $\langle\text{Ln-O}\rangle$ bonds [53–56, 68–73]. Spectra (figure 3) show that all compositions of rare-earth

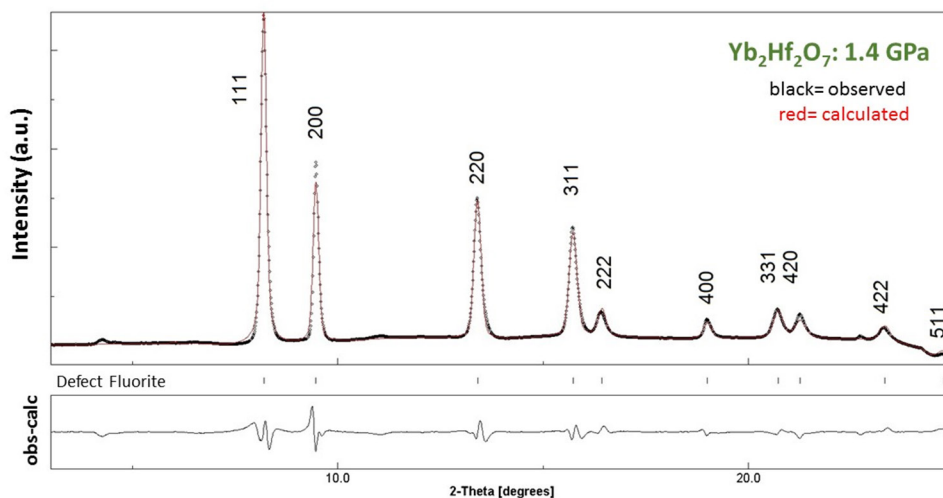


Figure 4. Indexed and refined diffraction pattern of $\text{Yb}_2\text{Hf}_2\text{O}_7$ (defect-fluorite) at 1.4 GPa. ($\lambda = 0.4959 \text{ \AA}$).

hafnates studied have an initial degree of pyrochlore-type short-range ordering of cations and oxygen vacancies. This is in agreement with recent experimental work by Popov *et al* [42, 43]; peak positions are consistent with previous theoretical and experimental Raman studies on rare-earth hafnates (table 2) [55, 57–60]. The first few modes at lower frequencies: F_{2g} , E_g , and F_{2g} modes arise from vibrations of the $\langle A-O \rangle$ and $\langle B-O \rangle$ bonds. The higher frequencies of F_{2g} arise from stretching of the $\langle B-O \rangle$ bonds. $\text{Sm}_2\text{Hf}_2\text{O}_7$, $\text{Eu}_2\text{Hf}_2\text{O}_7$, and $\text{Gd}_2\text{Hf}_2\text{O}_7$ show Raman spectra typical of pyrochlore-structured oxides [57–60, 68–73]. The four F_{2g} modes are evident and distinct, with the E_g and A_{1g} modes overlapping the first and third F_{2g} modes, respectively. The cation radius ratio (table 1) indicates that $\text{Dy}_2\text{Hf}_2\text{O}_7$, $\text{Yb}_2\text{Hf}_2\text{O}_7$, and $\text{Y}_2\text{Hf}_2\text{O}_7$ are expected to form defect-fluorite structures [41–43, 55]. However, Raman spectra for these compositions still show the six theoretical Raman-active modes for pyrochlore-structured oxides [57–60]. In a fully disordered defect-fluorite, individual modes would be indistinguishable; all the spectra here indicate some initial pyrochlore-type short-range ordering of cations and oxygen vacancies [57–60]. In spectra collected from all compositions, a 7th mode is evident around $\sim 750 \text{ cm}^{-1}$; this ‘breathing’ mode is attributed to distortions in the HfO_6 octahedra and is not strictly allowed in a perfect pyrochlore structure [57]. However, no defect-free pyrochlore exists, so this mode typically appears in spectra collected for all pyrochlore compositions [57].

Figure 4 shows an indexed and refined *in situ* diffraction pattern for characteristic defect-fluorite phase of hafnate $\text{Yb}_2\text{Hf}_2\text{O}_7$ at ~ 1.4 GPa. $\text{Yb}_2\text{Hf}_2\text{O}_7$ and $\text{Y}_2\text{Hf}_2\text{O}_7$ show typical diffraction patterns for the defect-fluorite structure at low pressures [1–11]. The XRD patterns for Dy-, Gd-, Eu-, and Sm- hafnates show a strong preferred orientation, with the (222) and (400) diffraction maxima having the highest intensity relative to other peaks. The preferred orientation may have been due to grain size, or interactions with the liquid pressure medium in the sample chamber. Nonetheless, for Gd-, Eu-, and Sm- hafnates, pyrochlore supercell peaks are evident, although with very low intensities (figure 5). *In situ* high-pressure XRD data from selected

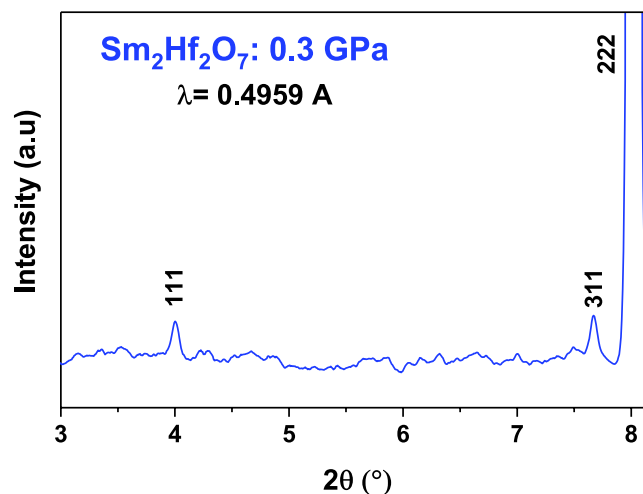


Figure 5. XRD graph of $\text{Sm}_2\text{Hf}_2\text{O}_7$ at 0.3 GPa, showing limited 2θ range and pyrochlore supercell diffraction maxima.

pressure points of representative compositions $\text{Gd}_2\text{Hf}_2\text{O}_7$, $\text{Dy}_2\text{Hf}_2\text{O}_7$, and $\text{Y}_2\text{Hf}_2\text{O}_7$ are shown in figure 6 (other compositions: figure S1.) A limited two-theta range is shown for $\text{Gd}_2\text{Hf}_2\text{O}_7$ and $\text{Dy}_2\text{Hf}_2\text{O}_7$ because of the preferred orientation; the strongest and most visible peaks are the (222) and (400) in $\text{Gd}_2\text{Hf}_2\text{O}_7$, and the (111) and (200) in $\text{Dy}_2\text{Hf}_2\text{O}_7$. A phase transition begins between 18 and 25 GPa for all compositions studied, evidenced by a broad band appearing between the (222) and (400) diffraction maxima; the intensity of this feature continues to grow while the pyrochlore and defect-fluorite peaks decrease in intensity up to pressures of ~ 50 GPa, the highest pressure studied. The slow phase transition to a cotunnite-like phase has been described before in zirconate pyrochlores and defect-fluorites [2–7, 11]. The new peak is assigned to the (120) maxima of the high-pressure phase. The phase transition in rare-earth hafnates takes place over 10–20 GPa (figure 7) and is still incomplete at ~ 50 GPa, the highest pressure examined for each composition. Figure 7 shows the progression of the phase transition using the relative intensities of the

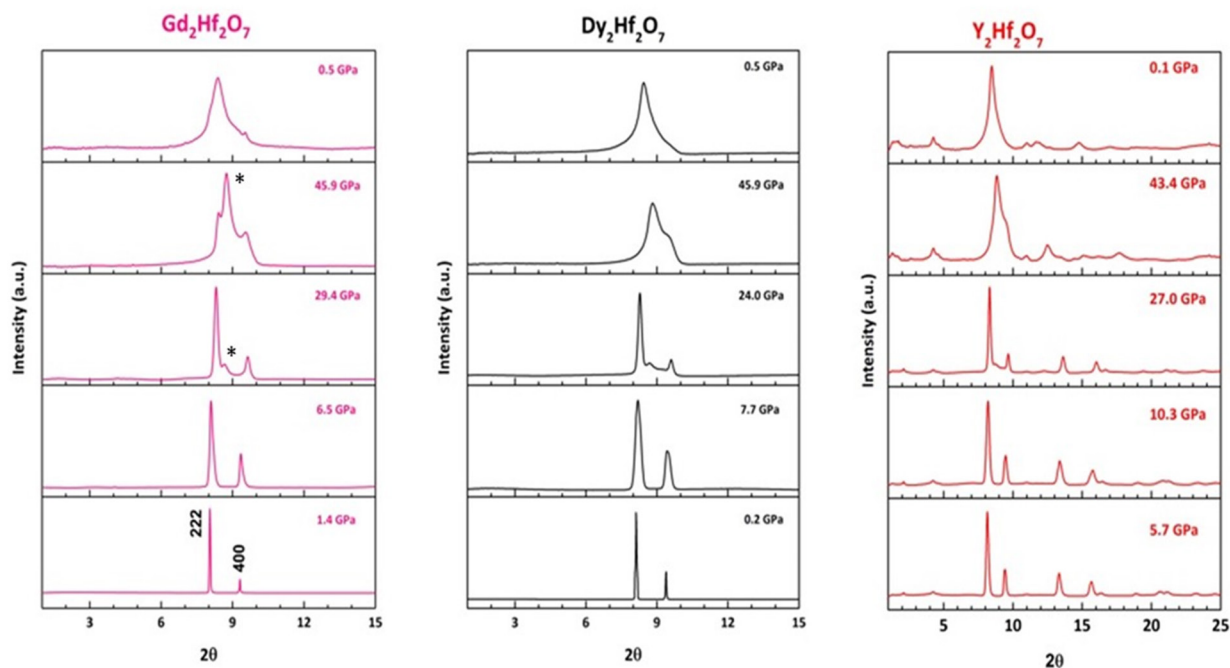


Figure 6. *In situ* high-pressure synchrotron x-ray diffraction patterns ($\lambda = 0.4959 \text{ \AA}$) of representative rare-earth hafnates with long-range ordered pyrochlore structure ($\text{Gd}_2\text{Hf}_2\text{O}_7$) and defect-fluorite structure ($\text{Dy}_2\text{Hf}_2\text{O}_7$, $\text{Y}_2\text{Hf}_2\text{O}_7$).

(120) cotunnite peak to the (222) pyrochlore peak. Data from $\text{Eu}_2\text{Hf}_2\text{O}_7$ are not shown because peak broadening and overlap prevents an accurate measurement of relative intensities. The phase transition in $\text{Sm}_2\text{Hf}_2\text{O}_7$ had progressed the least by 50 GPa relative to other compositions studied. After decompression to ambient pressure, $\text{Sm}_2\text{Hf}_2\text{O}_7$ showed distinct peaks from the defect-fluorite structure and peaks from the high-pressure cotunnite-like phase (figure S1). In the other compositions studied, XRD shows a relaxation to defect-fluorite type structure with an amorphous component as the samples are decompressed (figure 6). The XRD did not show any evidence of decomposition to A_2O_3 and HfO_2 , as was reported for $\text{La}_2\text{Hf}_2\text{O}_7$ [1].

P - V data for the pyrochlore or defect-fluorite phase of each composition were fit to a second-order Birch–Murnaghan equation of state (figure 8) [66]. The data from all pressure points were included unless peak broadening or overlap from the phase transition prevented an accurate (error > 0.009) refinement of the unit cell parameters of the pyrochlore or defect-fluorite phase. A mixture of methanol and ethanol in a 4:1 ratio was used as the pressure-transmitting medium. This mixture is hydrostatic until to ~ 11.5 GPa, but is quasi-hydrostatic above 11.5 GPa [61, 62]. In order to more accurately compare this study to previous studies on zirconate and titanate pyrochlores at high pressure [2–11], the B-M EOS was fit to all pressure-points possible (error in unit cell parameter < 0.01). The three pyrochlore compositions, $\text{Sm}_2\text{Hf}_2\text{O}_7$, $\text{Eu}_2\text{Hf}_2\text{O}_7$, and $\text{Gd}_2\text{Hf}_2\text{O}_7$ decrease in unit cell volume as the ionic radii of the lanthanides in the A-site decrease (table S2). Errors in B_0 and V_0 (table S2) were propagated from errors in the unit cell parameter at each pressure point. The bulk moduli for Eu- and Gd- hafnates are within error (15 GPa) of each other at approximately 240 GPa, with $\text{Sm}_2\text{Hf}_2\text{O}_7$ having a slightly

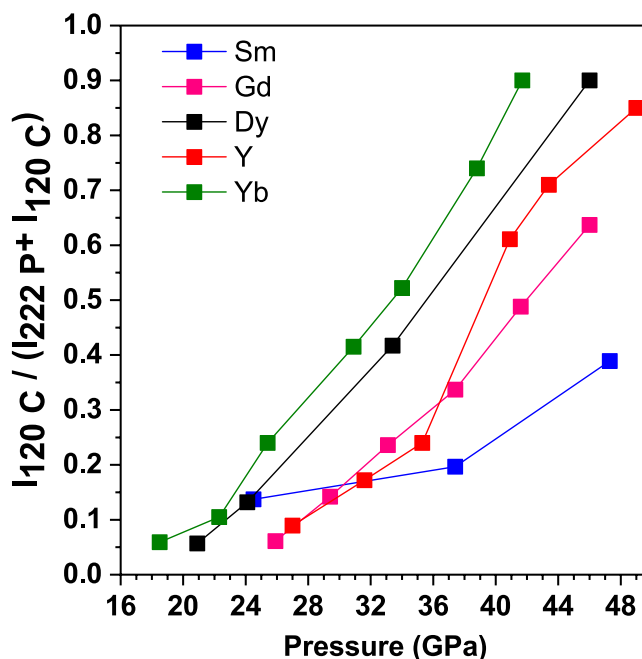


Figure 7. Relative intensity of most intense phase features: cotunnite maxima (120), to pyrochlore maxima (222) or defect-fluorite maxima (111), with increasing pressure after the onset of phase transition for Sm-, Gd-, Dy-, Y-, and Yb- hafnate compositions.

larger bulk modulus of 265 GPa (figure 9). For the defect-fluorite compositions of $\text{Dy}_2\text{Hf}_2\text{O}_7$, $\text{Yb}_2\text{Hf}_2\text{O}_7$, and $\text{Y}_2\text{Hf}_2\text{O}_7$, the ambient pressure unit cell volume is smallest in $\text{Yb}_2\text{Hf}_2\text{O}_7$, and similar for $\text{Dy}_2\text{Hf}_2\text{O}_7$ and $\text{Y}_2\text{Hf}_2\text{O}_7$. The bulk moduli of Y- and Yb- hafnates are within error (15 GPa) of each other at 400 GPa. $\text{Dy}_2\text{Hf}_2\text{O}_7$ has a noticeably lower bulk modulus of 303 GPa, although it has a comparable volume to $\text{Y}_2\text{Hf}_2\text{O}_7$

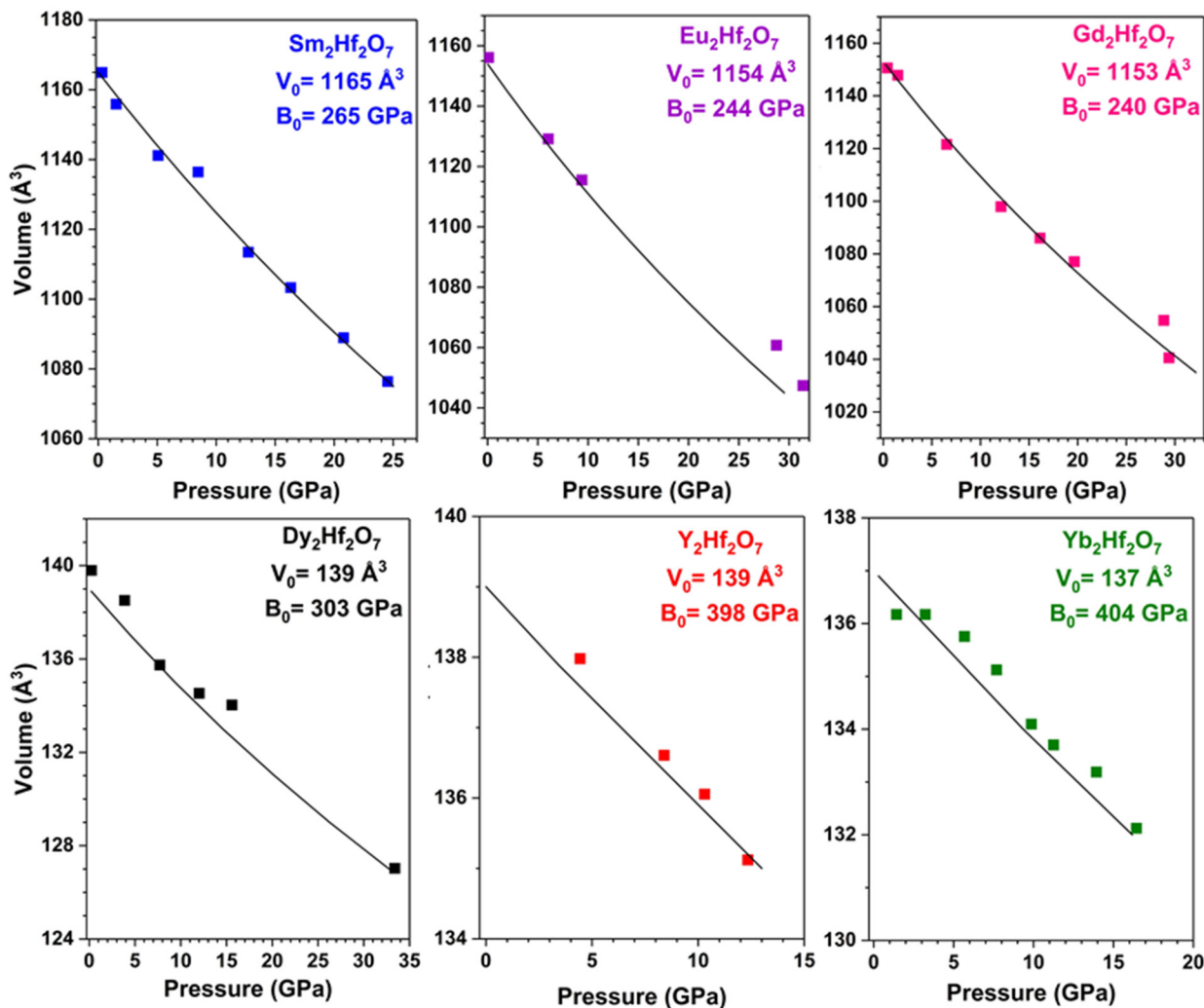


Figure 8. Second-order Birch–Murnaghan equation of state for rare-earth hafnates ($A_2Hf_2O_7$: A = Sm, Eu, Gd, Dy, Y, Yb).

and $Yb_2Hf_2O_7$. The trend of inversely correlated bulk modulus and radius ratio has been seen in zirconate and titanate pyrochlore oxides at high pressure [2–11]. Additionally, irradiated defect-fluorite oxides have shown a higher fracture toughness than pyrochlore-type oxides with the same B-cation, which is inversely related to the bulk modulus [74].

In situ high-pressure Raman spectroscopy of rare-earth hafnates shows several changes to the local structure (figure 10). Generally, pyrochlore-structured oxides and $Dy_2Hf_2O_7$ show distinct pyrochlore modes up to higher pressures (18–20 GPa) than defect-fluorite-structured $Y_2Hf_2O_7$ and $Yb_2Hf_2O_7$, of which the spectra quality is severely degraded at pressures as low as 4 GPa. $Sm_2Hf_2O_7$, $Eu_2Hf_2O_7$, and $Gd_2Hf_2O_7$ compositions have the largest cation radius ratio (table 1); in these materials, the pyrochlore Raman modes are evident and distinct until ~30–33 GPa. At the highest pressure measured (~50 GPa), a broad band between 200 and 300 cm^{-1} is evident in these compositions, which is attributed to the high-pressure cotunnite-like phase that pyrochlore is known to transform into [2]. For $Gd_2Hf_2O_7$, $Dy_2Hf_2O_7$, $Y_2Hf_2O_7$, and $Yb_2Hf_2O_7$, at the highest pressure (50 GPa) measured shows that the BO_6 ‘breathing mode’ [56] dominates the spectra around ~800 cm^{-1} .

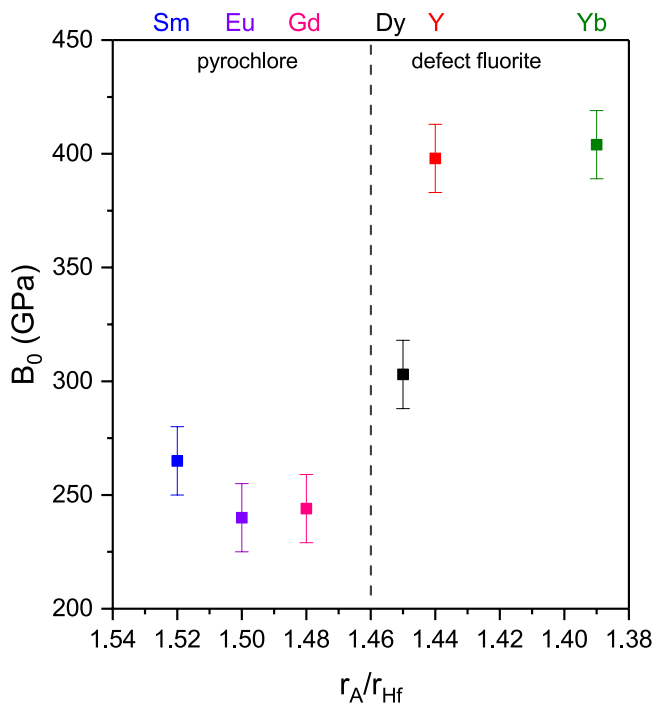


Figure 9. Bulk moduli of lanthanide hafnates from 2nd order Birch–Murnaghan equation of state [62].

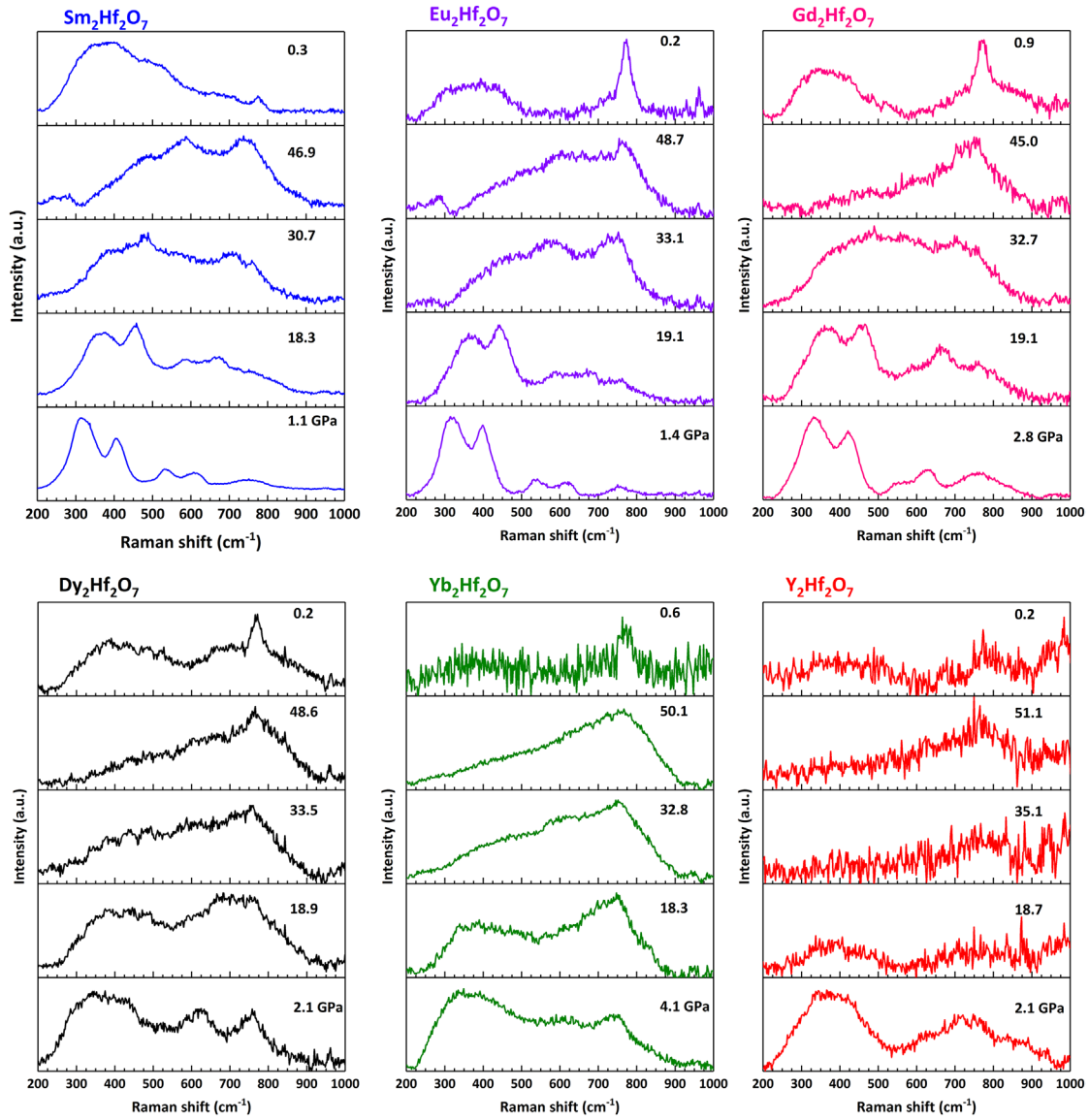


Figure 10. *In situ* high-pressure Raman spectra of rare-earth hafnates at selected pressures. Bottom four panels in each graph are materials under increasing compression. Top panel in each graph shows decompression from 50 GPa.

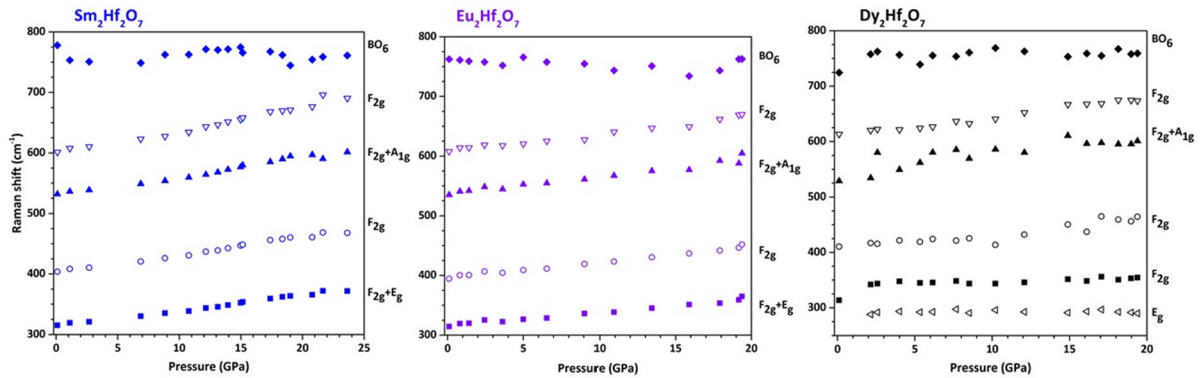


Figure 11. Peak positions of pyrochlore Raman-active modes with increasing pressure for rare-earth hafnates.

Figure 11 shows the increase in frequency versus pressure of the pyrochlore Raman-active modes and the BO_6 ‘breathing’ mode for $\text{Sm}_2\text{Hf}_2\text{O}_7$, $\text{Eu}_2\text{Hf}_2\text{O}_7$, and $\text{Dy}_2\text{Hf}_2\text{O}_7$ (other compositions, figure S2). The peaks shift

to increasing frequency with pressure and do not show discontinuities in slope below the onset pressure of the phase transition as indicated by x-ray diffraction data. Mode Grüneisen parameters [75] were calculated for each of the

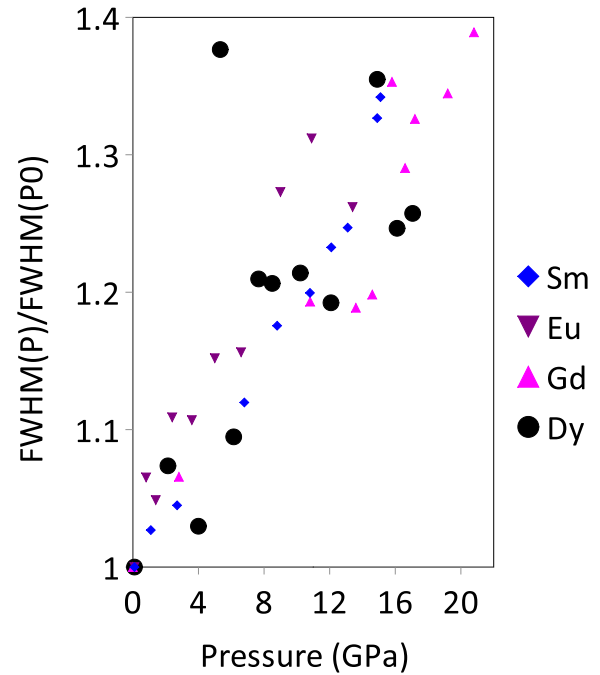
Table 3. Mode Grüneisen parameters for pyrochlore-type Raman-active modes of rare-earth hafnates.

Mode Grüneisen parameter; γ_{i0}						
A	Sm	Eu	Gd	Dy	Y	Yb
Mode						
$F_{2g}(+E_g)$	3.09	4.63	2.56	12.84	5.26	2.38
F_{2g}	2.65	4.48	3.03	2.20	0.05	0.31
$F_{2g} + A_{1g}$	2.00	3.29	1.74	1.45	10.64	11.94
F_{2g}	2.49	2.98	1.68	1.62	2.83	0.97
E_g (Dy, Y only)				8.43	11.62	

pyrochlore Raman-active modes (table 3). Generally, the mode Grüneisen parameters for pyrochlore-type hafnates (Sm-, Eu-, and Gd- hafnate) showed less variation relative to the defect-fluorite-type hafnates (Dy-, Y-, and Yb- hafnate).

Quenching to ambient pressure indicates differences between $\text{Sm}_2\text{Hf}_2\text{O}_7$ and all other compositions studied (figure 6). In quenched $\text{Sm}_2\text{Hf}_2\text{O}_7$, the modes of a pyrochlore-type material are present in the Raman spectra. The peaks are significantly broadened, suggesting the local structure of quenched $\text{Sm}_2\text{Hf}_2\text{O}_7$ is a defect-rich pyrochlore. For the other hafnate compositions, two bands are evident, centered around $\sim 350\text{cm}^{-1}$ and $\sim 800\text{cm}^{-1}$. The sharp ‘breathing mode’ around 800cm^{-1} is attributed to distortions of the BO_6 octahedra [56]. This modes’ appearance in the quenched Raman spectra indicates some cations in the structure are in octahedral coordination [12–14]. The band at $\sim 350\text{cm}^{-1}$ is assigned to a mixture of AO_8 and BO_6 vibrations that are separate modes in ordered pyrochlores. The broadened band indicates disorder in the quenched local structure. Spectra of this type have been reported previously in pyrochlores subjected to irradiation and high pressure, most recently in irradiated stannate pyrochlores that transformed to weberite-like structures [17]. It was recently discovered that the structure of disordered pyrochlores is best described as defect-fluorite-like at a long range— $> \sim 20\text{Å}$ — and weberite-like at a shorter range— $< \sim 20\text{Å}$ [38]. Hafnate pyrochlores quenched from 50 GPa indicate a defect-fluorite long-range structure by x-ray diffraction, and a weberite-like local structure by Raman spectroscopy. This could indicate that pyrochlore oxides disordered by compression have a similar pathway and structure to those disordered by irradiation and compositional defects [26].

The FWHM of the first peak— $F_{2g} + E_g$ —is used as a proxy for disordering of the local structure of pyrochlore; an increasing FWHM relative to FWHM at ambient pressure indicates increasing disorder with the formation of anion Frenkel-pairs and cation anti-site defects [42, 43]. The Raman-active modes in pyrochlore all correspond to stretching and bending vibrations in oxygen-cation bonds. Although Raman spectroscopy is more sensitive to the changes to the oxygen-sublattice than x-ray diffraction, disordering in the cation sublattice will also affect Raman modes. Sm-, Eu-, Gd-, and Dy- hafnates show a gradual increase of the FWHM of the first peak with pressure (figure 12), indicating that the onset of disorder in the material begins immediately as pressure is increased and then continues to gradually increase, which

**Figure 12.** Normalized full width at half maximum (FWHM) of $F_{2g} + E_g$ peak of hafnates (A = Sm, Eu, Gd, Dy) as a function of pressure.

is consistent with previous studies on pyrochlores at high pressures [2–11]. For Y- and Yb- hafnate, peaks overlap and broaden significantly even at pressures below 10 GPa; thus, FWHM peak analysis was not done.

Conclusions

In general, rare-earth hafnate pyrochlores and defect-fluorites show similar behavior to zirconates under high pressure [2–7, 11] as evidenced by *in situ* Raman spectroscopy and x-ray diffraction in DACs. Pyrochlore- and defect-fluorite-structured hafnates behave distinctly from each other under high pressures, though Raman spectroscopy at ambient conditions showed that all compositions initially had pyrochlore-type short range ordering (figure 3). *In situ* x-ray diffraction demonstrated that all compositions begin a slow phase transition to a cotunnite-like phase between 18 and 25 GPa that was not complete at 50 GPa (figure 6). After decompression, *in situ* x-ray diffraction demonstrated that all compositions quenched to defect-fluorite with an amorphous component (figure 6), rather than the $\text{Ln}_2\text{O}_3 + \text{HfO}_2$ observed for $\text{La}_2\text{Hf}_2\text{O}_7$ [1]. X-ray diffraction from pyrochlore-type hafnates and $\text{Dy}_2\text{Hf}_2\text{O}_7$ showed strong preferential orientation at high pressure, even under hydrostatic conditions. The Raman modes of pyrochlore-structured oxides were distinctly evident until pressures as high as 30 GPa; as compared with $\text{Dy}_2\text{Hf}_2\text{O}_7$ (18–20 GPa), $\text{Y}_2\text{Hf}_2\text{O}_7$, and $\text{Yb}_2\text{Hf}_2\text{O}_7$ (4 GPa). Compressibilities calculated from the 2nd order Birch–Murnaghan equation of state indicated that pyrochlore-type hafnates have a bulk modulus of $\sim 250\text{GPa}$, and defect-fluorite type hafnates have a bulk modulus of $\sim 400\text{GPa}$ (figure 9). Bulk moduli of hafnates are notably higher than analogous

zirconates and titanates [2–11], which may be due to the covalency of <Hf–O> bonds [76]

The behavior of Dy₂Hf₂O₇ was not entirely consistent with the other defect-fluorite hafnates studied at high pressure. Dy₂Hf₂O₇ showed preferential orientation, as revealed by x-ray diffraction, as did the pyrochlore-type hafnates. The pyrochlore-type Raman modes of Dy₂Hf₂O₇ persisted to significantly higher pressures than Y- and Yb-hafnates. The radius ratio of Dy₂Hf₂O₇ is similar to Y₂Hf₂O₇ (table 1). Furthermore, the compressibility of Dy₂Hf₂O₇ is an intermediate value ~300 GPa, suggesting the structure may be intermediate between that of pyrochlore and defect-fluorite. Recent work on the transition between pyrochlore and defect-fluorite in hafnates showed a similar result [42, 43]. The radius ratio of Dy₂Hf₂O₇ is just below the pyrochlore stability field, and its behavior at high pressures suggests hybrid influences of pyrochlore-short range ordering and the defect-fluorite long-range structure.

Recent work by Shamblin *et al* [38] has shown that fluorite and weberite-like structures coexist at different length scales in disordered pyrochlores, regardless of the disordering mechanism—irradiation, temperature, or compositional defects. Recent work by Tracy *et al* [17] showed irradiated stannate pyrochlore with a weberite-type local structure evidenced by Raman spectroscopy. The behavior of hafnate pyrochlore decompressed from 50 GPa suggests a similar result: a long-range structure best described as a defect-fluorite, with a weberite-like local structure.

Acknowledgments

This work was supported as part of the Materials Science of Actinides, an Energy Frontier Research Center funded by the US Department of Energy, Office of Science, Basic Energy Science under Award #DE-SC0001089. KMT gratefully acknowledges travel funding from the Stanford VPGE, EDGE-STEM program. Portions of this work were performed at HPCAT (Sector 16), Advanced Photon Source (APS), Argonne National Laboratory. HPCAT operations are supported by DOE-NNSA under Award No. DE-NA0001974 and DOE-BES under Award No. DE-FG02-99ER45775, with partial instrumentation funding by NSF. The Advanced Photon Source is a U.S. Department of Energy (DOE) Office of Science User Facility operated for the DOE Office of Science by Argonne National Laboratory under Contract No. DE-AC02-06CH11357. Portions of this work were performed at the Beamline 12.2.2 of the Advanced Light Source (ALS), Lawrence Berkeley National Laboratory. The ALS is a DOE Office of Science User Facility under contract no. DE-AC02-05CH11231. We thank the beamline scientists for their help: Martin Kunz (ALS), Changyong Park (APS), and Dmitri Popov (APS).

References

- [1] Garg N, Pandey K K, Murli C, Shanavas K V, Mandal B P, Tyagi A K and Sharma S M 2008 Decomposition of lanthanum hafnate at high pressures *Phys. Rev. B* **77** 214105
- [2] Rittman D R, Turner K M, Park S, Fuentes A F, Yan J, Ewing R C and Mao W L 2017 High-pressure behavior of A₂B₂O₇ pyrochlore (A = Eu, Dy; B = Ti, Zr) *J. Appl. Phys.* **121** 045902
- [3] Xiao H Y, Zhang F X, Gao F, Lang M, Ewing R C and Weber W J 2010 Zirconate pyrochlores under high pressure *Phys. Chem. Chem. Phys.* **12** 12472–7
- [4] Zhang F X, Lian J, Becker U, Ewing R C, Hu J and Saxena S K 2007 High-pressure structural changes in the Gd₂Zr₂O₇ pyrochlore *Phys. Rev. B* **76** 214104
- [5] Zhang F X, Lian J, Becker U, Wang L M, Hu J, Saxena S K and Ewing R C 2007 Structural distortions and phase transformations in Sm₂Zr₂O₇ pyrochlore at high pressures *Chem. Phys. Lett.* **441** 216–20
- [6] Zhang F X, Wang J W, Lian J, Lang M K, Becker U and Ewing R C 2008 Phase stability and pressure dependence of defect formation in Gd₂Ti₂O₇ and Gd₂Zr₂O₇ pyrochlores *Phys. Rev. Lett.* **100** 045503
- [7] Zhang F X, Lang M, Becker U, Ewing R C and Lian J 2008 High pressure phase transitions and compressibilities of Er₂Zr₂O₇ and Ho₂Zr₂O₇ *Appl. Phys. Lett.* **92** 011909
- [8] Zhang F X, Lang M, Tracy C L, Ewing R C, Gregg D J and Lumpkin G R 2014 Incorporation of uranium in pyrochlore oxides and pressure-induced phase transitions *J. Solid State Chem.* **219** 49–54
- [9] Zhang F X and Saxena S K 2005 Structural changes and pressure-induced amorphization in rare earth titanates RE₂Ti₂O₇ (RE: Gd, Sm) with pyrochlore structure *Chem. Phys. Lett.* **413** 248–51
- [10] Zhang F X, Manoun B and Saxena S K 2006 Pressure-induced order—disorder transitions in pyrochlore: Re₂Ti₂O₇ (Re = Y, Gd) *Mater. Lett.* **60** 2773–6
- [11] Zhang F X, Lang M, Liu Z and Ewing R C 2010 Pressure-induced disordering and anomalous lattice expansion in a La₂Zr₂O₇ pyrochlore *Phys. Rev. Lett.* **105** 015503
- [12] Maczka M, Sanjuan M L, Fuentes A F, Hermanowicz K and Hanuza J 2008 Temperature-dependent Raman study of the spin-liquid pyrochlore Tb₂Ti₂O₇ *Phys. Rev. B* **78** 134420
- [13] Maczka M, Sanjuan M L, Fuentes A F, Macalik L, Hanuza J, Matsuhira K and Hiroi Z 2009 Temperature-dependent studies of the geometrically frustrated pyrochlores Ho₂Ti₂O₇ and Dy₂Ti₂O₇ *Phys. Rev. B* **79** 214437
- [14] Sanjuan M L, Guglieri C, Diaz-Moreno S, Aquilanti G, Fuentes A F, Olivi L and Chaboy J 2011 Raman and x-ray absorption spectroscopy study of the phase evolution induced by mechanical milling and thermal treatments in R₂Ti₂O₇ pyrochlores *Phys. Rev. B* **84** 104207
- [15] Zhang F X, Lang M and Ewing R C 2015 Atomic disorder in Gd₂Zr₂O₇ pyrochlore *Appl. Phys. Lett.* **106** 191902
- [16] Shamblin J, Tracy C L, Ewing R C, Xhang F, Li W, Trautmann C and Lang M 2016 Structural response of titanate pyrochlores to swift heavy ion irradiation *Acta Mater.* **117** 207–15
- [17] Tracy C L, Shamblin J, Park S, Zhang F, Trautmann C, Lang M and Ewing R C 2016 Role of composition, bond covalency, and short-range order in the disordering of stannate pyrochlores by swift heavy ion irradiation *Phys. Rev. B* **94** 064102
- [18] Lang M, Devanathan R, Toulemonde M and Trautmann C 2015 Advances in understanding of swift heavy-ion tracks in complex ceramics *Curr. Opin. Solid State Mater. Sci.* **19** 39–48
- [19] Park S, Lang M, Tracy C L, Zhang J, Zhang F, Trautmann C, Rodriguez M D, Kluth P and Ewing R C 2015 Response of Gd₂Ti₂O₇ and La₂Ti₂O₇ to swift-heavy ion irradiation and annealing *Acta Mater.* **93** 1–11
- [20] Lang M *et al* 2015 Characterization of ion-induced radiation effects in nuclear materials using synchrotron x-ray techniques *J. Mater. Res.* **30** 1366–79

- [21] Zhang J, Toulemonde M, Lang M, Costantini J M, Della-Negra S and Ewing R C 2015 C_{60} and U ion irradiation of $Gd_2Ti_xZr_{2-x}O_7$ pyrochlore *J. Mater. Res.* **30** 2456–66
- [22] Skuratov V A, Sohatsky A S, O'Connell J H, Kornieieva K, Nikitina A A, Neethling J H and Ageev V S 2015 Swift heavy ion tracks in $Y_2Ti_2O_7$ nanoparticles in EP450 ODS steel *J. Nucl. Mater.* **456** 111–4
- [23] Lang M *et al* 2014 Swift heavy ion track formation in $Gd_2Zr_{2-x}Ti_xO_7$ pyrochlore: effect of electronic energy loss *Nucl. Instrum. Methods Phys. Res. B* **336** 102–15
- [24] Park S, Lang M, Tracy C L, Zhang J, Zhang F, Trautmann C, Kluth P, Rodriguez M D and Ewing R C 2014 Swift heavy ion irradiation-induced amorphization of $La_2Ti_2O_7$ *Nucl. Instrum. Methods Phys. Res. B* **326** 145–9
- [25] Wang J, Lang M, Ewing R C and Becker U 2013 Multi-scale simulation of structural heterogeneity of swift-heavy ion tracks in complex oxides *J. Phys.: Condens. Matter* **25** 1–14
- [26] Lang M, Zhang F, Zhang J, Wang J, Lian J, Weber W J, Schuster B, Trautmann C, Neumann R and Ewing R C 2010 Review of $A_2B_2O_7$ pyrochlore response to irradiation and pressure *Nucl. Instrum. Methods Phys. Res. B* **268** 2951–9
- [27] Zhang J, Lang M, Ewing R C, Devanathan R, Weber W J and Toulemonde M 2010 Nanoscale phase transitions under extreme conditions within an ion track *J. Mater. Res.* **25** 1344–51
- [28] Lang M, Lian J, Zhang J, Zhang F, Weber W J, Trautmann C and Ewing R C 2009 Single-ion tracks in $Gd_2Zr_{2-x}Ti_xO_7$ pyrochlores irradiated with swift heavy ions *Phys. Rev. B* **79** 224105
- [29] Lang M, Zhang F, Zhang J, Wang J, Schuster B, Trautmann C, Neumann R, Becker U and Ewing R C 2009 Nanoscale manipulation of the properties of solids at high pressure with relativistic heavy ions *Nat. Mater.* **8** 793–7
- [30] Zhang J *et al* 2009 Enhanced radiation resistance of nanocrystalline pyrochlore $Gd_2(Ti_{0.65}Zr_{0.35})_2O_7$ *Appl. Phys. Lett.* **94** 243110
- [31] Zhang J, Lian J, Fuentes A F, Zhang F, Lang M, Lu F and Ewing R C 2009 Liquid-like phase formation in $Gd_2Zr_2O_7$ by extremely ionizing irradiation *J. Appl. Phys.* **105** 113510
- [32] Lang M, Zhang F, Lian J, Trautmann C, Neumann R and Ewing R C 2009 Combined high pressure and heavy-ion irradiation: a novel approach *J. Synchrotron Irradiat.* **16** 773–7
- [33] Sattonnay G, Moll S, Thome L, Legros C, Herbst-Ghysel M, Garrido F, Costantini J M and Trautmann C 2008 Heavy-ion irradiation of pyrochlore oxides: comparison between low and high energy regimes *Nucl. Instrum. Methods Phys. Res. B* **266** 3043–7
- [34] Sattonnay G, Moll S, Thome L, Legros C, Calvo A, Herbst-Ghysel M, Decorse C and Monnet I 2012 Effect of composition on the behavior of pyrochlores irradiated with swift heavy ions *Nucl. Instrum. Methods Phys. Res. B* **272** 261–5
- [35] Sattonnay G, Sellami N, Thome L, Legros C, Grygiel C, Monnet I, Jagielski J, Jozwik-Biala I and Simon P 2013 Structural stability of $Nd_2Zr_2O_7$ pyrochlore ion-irradiated in a broad energy range *Acta Mater.* **61** 6492–505
- [36] Soulie A, Menu D, Crocombette J P, Chartier A, Sellami N, Sattonnay G, Monnet I and Bechade J L 2016 X-ray diffraction study of the $Y_2Ti_2O_7$ pyrochlore disordering sequence under irradiation *J. Nucl. Mater.* **480** 314–22
- [37] Sattonnay G *et al* 2016 Key role of the short-range order on the response of the titanate pyrochlore $Y_2Ti_2O_7$ to irradiation *Phys. Rev. B* **94** 224109
- [38] Shamblin J, Feyngenson M, Neuefeind J, Tracy C L, Zhang F, Finkeldei S, Bosbach D, Zhou H, Ewing R C and Lang M 2016 Probing disorder in isometric pyrochlore and related complex oxides *Nat. Mater.* **15** 507–11
- [39] Tracy C L, Lang M, Zhang F, Park S, Palomares R I and Ewing R C 2016 Review of recent experimental results on the behavior of actinide-bearing oxides and related materials in extreme environments *Prog. Nucl. Energy* 1–17
- [40] Ewing R C, Weber W J and Lian J 2004 Nuclear waste disposal—pyrochlore ($A_2B_2O_7$): nuclear waste form for the immobilization of plutonium and 'minor' actinides *J. Appl. Phys.* **95** 5949
- [41] Subramanian M A, Aravamudan G and Subba Rao G V 1983 Oxide pyrochlores—a review *Prog. Solid State Chem.* **15** 55–143
- [42] Popov V, Menushenkov A P, Yastrebtshev A A and Zubavichus Y V 2016 $La_2Hf_2O_7$ crystal and local structure changes on the fluorite-pyrochlore phase transition *J. Phys.: Conf. Ser.* **747** 012043
- [43] Popov V, Menushenkov A P, Yaroslavtsev A A, Zubavichus Y V, Gayanov B R, Yastrebtshev A A, Leshchev D S and Chernikov R V 2016 Fluorite-pyrochlore phase transition in nanostructured $Ln_2Hf_2O_7$ ($Ln = La-Lu$) *J. Alloys Compd.* **689** 669–79
- [44] Minervini L and Grimes R W 2000 Disorder in pyrochlore oxides *J. Am. Ceram. Soc.* **83** 1873–8
- [45] Minervini L, Grimes R W, Tabira Y, Withers R L and Sickafus K E 2002 The oxygen positional parameter in pyrochlores and its dependence on disorder *Phil. Mag. A* **82** 123–35
- [46] Moriga T, Yoshiasa A, Kanamaru F, Koto K, Yoshimura M and Somiya S 1988 Crystal Structure analyses of the pyrochlore and fluorite-type $Zr_2Gd_2O_7$ and phase domain structure *Solid State Ion.* **31** 319–28
- [47] Pirzada M, Grimes R W, Minervini L, Maguire J F and Sickafus K E 2001 Oxygen migration in $A_2B_2O_7$ pyrochlores *Solid State Ion.* **140** 201–8
- [48] van Dijk M P, de Vries K J and Burggraaf A J 1983 Oxygen ion and mixed conductivity in compounds with the fluorite and pyrochlore structure *Solid State Ion.* **9** 913–20
- [49] Wilde P J and Catlow C R A 1998 Defects and diffusion in pyrochlore structured oxides *Solid State Ion.* **112** 173–83
- [50] Lian J, Wang L, Chen J, Sun K, Ewing R C, Farmer J M and Boatner L A 2003 The order—disorder transition in ion-irradiated pyrochlore *Acta Mater.* **51** 1493–502
- [51] Wang S X, Wang L M, Ewing R C, Was G S and Lumpkin G R 1999 Ion-irradiation-induced phase transformation of pyrochlore and zirconolite *Nucl. Instrum. Methods Phys. Res. B* **148** 704–9
- [52] Sattonnay G, Moll S, Thome L, Decorse C, Legros C, Simon P, Jagielski J, Jozwik I and Monnet I 2010 Phase transformations induced by high electronic excitation in ion-irradiated $Gd_2(Zr_xTi_{1-x})_2O_7$ pyrochlores *J. Appl. Phys.* **108** 103512
- [53] Lian J, Zu X T, Kutty K V G, Chen J, Wang L M and Ewing R C 2002 Ion-irradiation-induced amorphization of $La_2Zr_2O_7$ pyrochlore *Phys. Rev. B* **66** 054108
- [54] Solomon J M, Shamblin J, Lang M, Navrotsky A and Asta M 2016 Chemical ordering in substituted fluorite oxides: a computational investigation of $Ho_2Zr_2O_7$ and $Re_2Th_2O_7$ ($RE = Ho, Y, Gd, Nd, La$) *Sci. Rep.* **6** 1–9
- [55] Stanek C R and Grimes R W 2002 Prediction of rare earth $A_2Hf_2O_7$ pyrochlore phases *J. Am. Ceram. Soc.* **86** 2139–41

- [56] Lopez-Cota F A, Cepeda-Sanchez N M, Diaz-Guillen J A, Dura O J, Lopez de la Torre M A, Maczka M, Ptak M and Fuentes A F 2017 Electrical and thermophysical properties of mechanochemically obtained lanthanide hafnates *J. Am. Ceram. Soc.* 1–11
- [57] Blanchard P E R, Liu S, Kennedy B J, Ling C D, Avdeev M, Aitken J B, Cowie B C C and Tadich A 2013 Investigating the local structure of lanthanoid hafnates $\text{Ln}_2\text{Hf}_2\text{O}_7$ via diffraction and spectroscopy *J. Phys. Chem.* **115** 2266–73
- [58] Mandal B P, Garg N, Sharma S M and Tyagi A K 2006 Preparation, XRD, and Raman spectroscopic studies on new compounds $\text{RE}_2\text{Hf}_2\text{O}_7$ (RE = Dy, Ho, Er, Tm, Lu, Y): pyrochlores or defect-fluorite? *J. Solid State Chem.* **179** 1990–4
- [59] Gupta H C, Brown S, Rani N and Gohel V B 2002 A lattice dynamical investigation of the Raman and the infrared frequencies of the cubic $\text{A}_2\text{Hf}_2\text{O}_7$ pyrochlores *J. Phys. Chem. Solids* **63** 535–8
- [60] Kumar S and Gupta H C 2012 First principles study of dielectric and vibrational properties of pyrochlore hafnates *Solid State Sci.* **14** 1405–11
- [61] Piermarini G J, Block S and Barnett J D 1973 Hydrostatic limits in liquids and solids to 100 kbar *J. Appl. Phys.* **44** 5377–82
- [62] Angel R, Bujak M, Zhao J, Gatta G D and Jacobsen S D 2007 Effective hydrostatic limits of pressure media for high-pressure crystallographic studies *J. Appl. Crystallogr.* **40** 26–32
- [63] Mao H K, Bell P M, Shaner J W and Steinberg D J 1978 Specific volume measurements of Cu, Mo, Pd, and Ag and calibration of the ruby R1 fluorescence pressure gauge from 0.06 to 1 Mbar *J. Appl. Phys.* **49** 3276–83
- [64] Wojdyr M 2010 Fityk: a general-purpose peak fitting program *J. Appl. Crystallogr.* **43** 1126–8
- [65] Lutterotti L, Matthies S and Wenk H R 1999 MAUD: a friendly Java program for material analysis using diffraction *IUCr: Newsl. CPD* **21** 14–5
- [66] Birch F 1947 Finite elastic strain of cubic crystals *Phys. Rev.* **71** 809
- [67] Angel R, Alvaro M and Gonzalez-Platas J 2014 EosFit7c and a Fortran module (library) for equation of state calculations *Z. Kristallogr. Cryst. Mater.* **229** 405–19
- [68] Vandendorre M T and Husson E 1983 Comparison of the force field in various pyrochlore families. I. The $\text{A}_2\text{B}_2\text{O}_7$ Oxides *J. Solid State Chem.* **50** 362–71
- [69] Vandendorre M T and Husson E 1984 Comparison of the force field in various pyrochlore families II. Phases presenting structural defects *J. Solid State Chem.* **53** 253–9
- [70] Vandendorre M T, Husson E, Chatry J P and Michel D 1983 Rare-earth titanates and stannates of pyrochlore structure; vibrational spectra and force fields *J. Raman Spectrosc.* **14** 63–71
- [71] Scheetz B E and White W B 1983 Temperature-dependent Raman spectra of rare-earth titanates with the pyrochlore structure: a dipolar order-disorder transition *Opt. Eng.* **22** 223302
- [72] Poulsen F W, Glerup M and Holtappels P 2000 Structure, Raman spectra and defect chemistry modelling of conductive pyrochlore oxides *Solid State Ion.* **135** 595–602
- [73] Saha S *et al* 2006 High-pressure Raman and x-ray study of the spin-frustrated pyrochlore $\text{Gd}_2\text{Ti}_2\text{O}_7$ *Phys. Rev. B* **74** 064109
- [74] Sattonay G, Moll S, Desbrosses V, Menvie Bekale V, Legros C, Thome L and Monnet I 2010 Mechanical properties of fluorite-related oxides subjected to swift-ion irradiation: pyrochlore and zirconia *Nucl. Instrum. Methods Phys. Res. B* **268** 3040–3
- [75] Sherman W F 1982 Pressure-induced changes in mode Grüneisen parameters and general equations of state for solids *J. Phys. C: Solid State Phys.* **15** 9–23
- [76] Gao F, He J, Wu E, Liu S, Yu D, Li D, Zhang S and Tian Y 2003 Hardness of covalent crystals *Phys. Rev. Lett.* **91** 015502